Optic disc localization using graph traversal algorithm along blood vessel in polar retinal image

Annupan Rodtook[1], Sirikan Chucherd[2]
[1]Department of Computer Science, Faculty of Science, Ramkhamheang University, Bangkok, Thailand
[2]Center of Excellence in AI and Emerging Technology, School of Information Technology, Mae Fah Luang University, Chiang Rai, Thailand

Article Info

ABSTRACT

The optic disc (OD) is an important landmark of the retina and its location is essential for computer-aided diagnosis of diabetic retinopathy and glaucoma. This paper presented a new method that applies the proposed graph traversal algorithm for vertical vascular infrastructure to detect root nodes representing the location of optical discs. The proposed algorithms were designed to process the terrific view of blood vessels from a polar image without depending on the prominent OD characteristic of circular/elliptical shape and brightness. Before constructing the vascular infrastructure, the new multi-scale and multi-orientation top-hat filters were proposed to properly approximate blood vessels of different sizes and directions. The proposed method provided efficiency and certainty for complex retinal images such as low contrast OD with low illumination and distorted OD shape due to complex vascular structure. The algorithms evaluation was performed on five public fundus image databases for retinal image analysis. Experimental results revealed that the proposed algorithm identified valid optical discs with high accuracy as 91.21%, 95.09%, 88.45%, 91.66%, and 95.01% for the five corresponding data sets and outperformed comparison methods.

Corresponding Author:

Sirikan Chucherd
Center of Excellence in AI and Emerging Technology, School of Information Technology
Mae Fah Luang University
Chiang Rai, Thailand
Email: sirikan@mfu.ac.th

1. INTRODUCTION

Testing for retinal disease in a computer-based manner is an important step in helping an ophthalmologist make a diagnosis. This not only saves time and resources, but also guarantees excellent accuracy. Diabetic retinopathy, glaucoma, hemorrhages, drusen, and arterial hypertension are examples of retinal disease. Especially diabetic retinopathy, which is the leading cause of vision loss according to the 2016 global record [1]. Consequently, more pertinent eye information aids in professional diagnosis. Therefore, the faster the diagnosis of the disease, the more effective the treatment. The optic disc (OD) is one of the main elements for displaying eye information. The greatest brilliant yellowish color region in the central half of the retinal image represents the typical OD. The OD has been employed as a starting point in the study of retinal pictures because of its unique properties. Many characteristics of the OD, including form, size, color, intensity, and location, can be used to monitor the eye disorders. An accurate OD localization is needed to reduce false positives in the diagnosis of eye disease. As a reason, detecting an anomaly or eye disease at an early stage can assist prevent visual impairment.

Many researchers are motivated to grow and develop a variety of concepts for a better automated evaluation system because of the high accuracy of the diagnosis. In the recent decade, kinds of literature on automated OD detection have been proposed with varying degrees of success. Many approaches have been proposed based on shape, size, intensity, and vascular structure. The OD was detected using characteristics such as a circle or elliptical shape and size. The circular-like characteristic underpins the proposed concept. To estimate image intensity variation related to the OD, the operator in [2] was oriented with certain angles and pixel length. Meanwhile, to obtain the shape and image variation around the boundary, a circular transformation was used [3]. Finally, the maximum/minimum variation value had been used to forecast the OD region. In addition, the OD size and edge information were employed to identify the potential pixels. The OD border was identified in [4] using hybrid level set segmentation, least square ellipse fitting, and adaptive template matching at various picture resolutions. However, to be the candidate pixels, Xiong and Li [5] merged the OD edge with vessel information from a region-of-interest (ROI). Finally, the candidate list was used to determine the confidence score for the exact OD. Moreover, the OD intensity and color-based detection methods had been proposed by various research groups. Zou *et al.* [6] provided the image intensity to create the OD candidate region first. Finally, when the model validated the result area, this location was determined as the OD center. Gutierrez *et al.* [7], the OD segmentation was proposed based on Markowitz's modern portfolio theory. Each color channel's optimal weights were calculated by the model. Then, a color fusion model was used to segment the OD. On the other hand, Gui *et al.* [8] applied corner detection technology to avoid location errors due to inaccurate subdivision of brightness and blood vessels. Instead, it was proposed that edge and gray information be considered. Next, the discovery window and the number of corner points were determined. The OD position, finally, was the center with the most corner points. Also, Nergiz *et al.* [9] used the color combined with the signs of primary vessels to identify OD. The convergence of the blood arteries first used to get a rough area of the OD. Next, a fuzzy logic controller (FLC) was provided to identify the exact OD center.

OD was localized using not only the above features but also the optic nerve convergence analysis. This is because OD is the area where blood vessels and nerves are concentrated in the retina. Therefore, retinal vessel segmentation was an important process in OD localization in [10]. Over the last decade, many retinal vascular segmentation systems had been proposed. Hoover *et al.* [11], the morphological filtering and region growing technique were proposed. Sun *et al.* [12] performed a wavelet transform, morphology, and the k-means clustering algorithm to classify the blood vessels and backgrounds. Meanwhile [13] applied high-pass filtering, a pixel neighborhood and a gradient image to classify major vessel pixels. Wang *et al.* [14] proposed a semi-supervised machine learning method that uses a cascade classification framework for retinal vessel segmentation.

Compared to previous frameworks, most of their solutions provided accurate results on normal retinal images. However, given the complex structure of OD in retinal images, most of these techniques did not work well. Here are some examples of different situations: i) due to the disorder of the vascular structure, the OD structure is not displayed as a circle or an ellipse, ii) The shape of OD is partially spherical due to improper field of view (FOV), and iii) the appearance of OD and some adjacent diseases (exudate and drusen) are similar in shape, size, and brightness. Due to these issues, OD detection algorithms based on the brightness and shape of the bright spot area may be less effective. Many researchers in the field of OD detection still faced difficult challenges due to these discrepancies.

This study paves the way for OD localization from retinal images with varieties of obstacles. The proposed procedure is based on the intersection area of the optic nerve and the ophthalmic artery examination. It appears as a long arc that resembles the letter C. The main purpose of this study is to detect the C band, which includes the arteries, veins, nerves, and optic discs of the eye. Before segmenting the blood vessels, polar image transformation transforms the vasculature from a parabola to a vertical curve. In this study, blood vessels of various sizes and orientations are properly preserved by a new and improved top-hat filter. The pruning procedure is performed on histogram images of bifurcation and crossing patterns, narrowing the perimeter of the ophthalmic artery and removing the capillaries (in cartesian coordinates) that represent the C band of the retinal vessels. Graph traversal algorithm along the blood vessel was proposed to find the node with the highest score, which represents the location of the optic disc where the central retinal artery originates from the optic disc.

The following sections of the paper are organized as follows: a theoretical framework, a proposed model for locating the optic disc of preliminary examples and the content. Section 3 exposes and discusses the approach performance parameters as well as the experimental outcomes of our model when compared to other models employing performance analysis. The conclusion is presented in section 4.

2.   THEORETICAL FRAMEWORK
2.1. The polar image transforms
Polar image transformation [15] is a well-known method for unpacking round object images (Figure 1(a)) into linear images (see Figures 1(b) and 1(c)). Image components with parabolic or curvilinear

curves surrounding the reference point are converted to horizontal or vertical curves. In this study, algorithms were designed to perform segmentation of the optic nerve, central retinal artery, branch retinal vein and ophthalmic artery on polar images. In mathematics, a point in the polar coordinate system is given as $f(r, \theta)$.

$$r = \sqrt{(x - x_c)^2 + (y - y_c)^2)} \tag{1}$$

$$\theta = \tan^{-1}\left(\frac{y - y_c}{x - x_c}\right) \tag{2}$$

where r known as the radial coordinate is the distance between the point (x, y) and the pole (x_c, y_c) and described on the unit circle that $0 \leq r \leq 1$, as in (1). Whereas θ is the angle between the point and the fixed direction, as in (2).
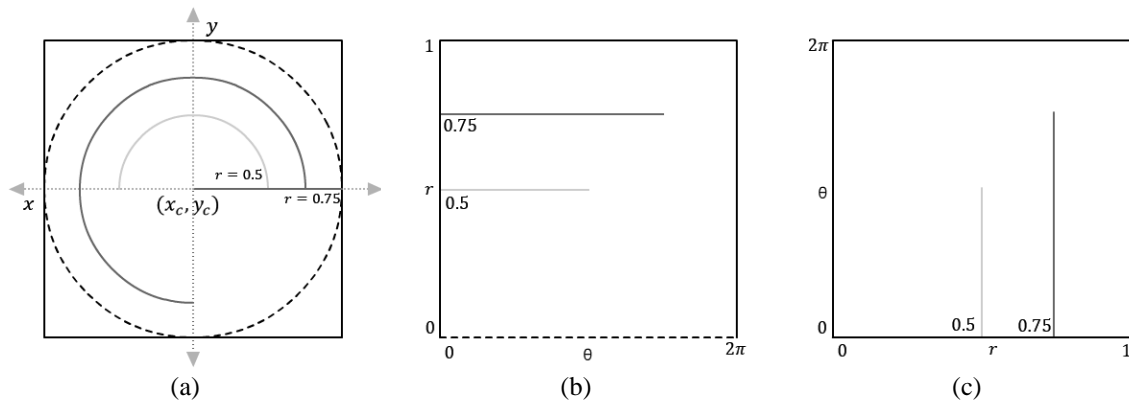

Figure 1. Coordinate system (a) cartesian (x, y), (b) polar $f(r, \theta)$, and (c) polar $f(\theta, r)$

2.2. Blood vessel approximation

The top hat filter is a popular operation for extracting targets from image and is used to approximate blood vessels on this research. However, the size and orientation of the blood vessels affect the completeness of the results. Therefore, this research proposed the multi-scale and multi-orientation top hat filter to approximate the retinal vasculature consisting of the optic nerve segment, the central retina and the ophthalmic artery. The modified version as in (3) and (4) (Figure 2(a)) is given by:

$$I_{i+1} = \left(I_i \circ e_{ij}\right) \bullet e_{ij}; i = 0, 1, \dots, k - 1; j = 0, 1, 2, 3 \tag{3}$$

$$T(I) = I_0 - I_k \tag{4}$$

T is a top-hat function where I_0 and e_{ij} are an initial image and elliptical morphological structural elements. The parameters i and j are scale and rotation indexes. The set of $\{e_i\}$ consists of scale-adaptive structural elements. The scale provides a sequence of structural elements that are rotated to different degrees $\left(rot(e_i, 0), rot(e_i, \frac{\pi}{4}), rot(e_i, \frac{\pi}{2}), rot(e_i, \frac{3\pi}{4})\right)$ (Figures 2(b) and 2(c)) to construct top hat filters for blood vessels of different sizes and orientations. In (3), the repeated opening operation (∘) removes blood vessels with adaptive elliptical structural elements e_{ij}, and the closing operation (•) suppresses residual noise due to inadequate opening structural elements.

2.3. Corner detection

In this research, corner detection is beneficial in characterizing branching and crossing patterns of blood vessels. It works on the principle of the pixel's intensity distinctness inside a given window. At a corner, the pixel is maintained with intensity variation in most directions. The measurement of intensity variation based on the Harris approach [8] is given by (5) and (6) as follows,

$$E(x, y) = \sum_{u,v} w(u, v)\left(f(x + u, y + v) - f(x, y)\right)^2 \tag{5}$$

$E(x, y)$ is an intensity differentiation within a window centred at pixel (x, y) and then shift point by (u, v) along the horizontal and vertical directions. $w(u, v)$ is the Gaussian coefficients calculated by:

$$w(u,v) = \frac{1}{2\pi\sigma^2} exp\left(-\frac{u^2+v^2}{2\sigma^2}\right) \tag{6}$$

the (7) presents the Taylor expansion of $E(x,y)$ in the linearization equation.

$$E(x,y) = \sum_{u,v} w(u,v)\left(I_x^2 u^2 + I_y^2 v + 2I_x I_y\right) \tag{7}$$

Then, the equation is rewritten in term of matrix operation in the form $E(x,y) = [u \quad v]M\begin{bmatrix}u\\v\end{bmatrix}$ which the Harris matrix (M) is constructed by (8).

$$M = \begin{pmatrix} \sum_{u,v} w(u,v)I_x^2 & \sum_{u,v} w(u,v)I_x I_y \\ \sum_{u,v} w(u,v)I_x I_y & \sum_{u,v} w(u,v)I_y^2 \end{pmatrix} \tag{8}$$

Let I_x and I_y be the partial derivatives of $I(x,y)$. Finally, $R(x,y)$ as in (9) is an eigenvalue equation for measuring corner characteristics as:

$$R(x,y) = det(M) + \alpha\big(trace(M)\big)^2 \tag{9}$$

where $det(M) = \lambda_1\lambda_2$ and $trace(M) = \lambda_1+\lambda_2$. Let λ_1 and λ_2 be the eigenvalues of M while α is the weighting coefficient.
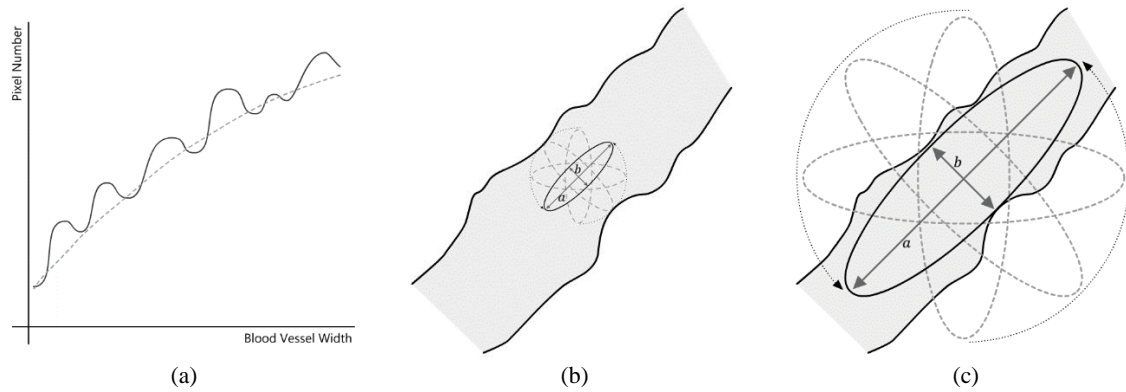

Figure 2. Coordinate system (a) the multi-scale and multi-orientation top-hat filters, (b) and (c) adaptive scale and orientation of the elliptical structural elements, (b) smaller scale structural elements, and (c) larger scale structural elements

In Figure 3, the solid black outline shows significant changes in all directions producing a large R that occurs when λ_1 and λ_2 are large and $\lambda_1 \sim \lambda_2$. In the case of significant changes in some directions of the bend or curve (the solid grey outline), R score is neither too high nor too low. When $R < 0$ and $\lambda_1 \gg \lambda_2$, this shows that there is no change along the edge direction (the grey dash outline).

Figure 3. Corner detection of blood vessel

2.4. The graph traversal algorithm

This section presents a graph traversal algorithm in which graph nodes identify branching and intersecting patterns, including vascular ends. This algorithm consists of traversing the graph and calculating the scores of the graph nodes. Based on the symmetry of the retinal vessels, the highest node score is used to discover the root of the vessel where the central retinal artery radiates from the optic nerve head. The algorithm starts with the contour tracing module carried out to the vertical vascular infrastructure [16] (Figure 4(a)) (see in appendix) for simulating a graph inclusive of nodes and edges (Figure 4(b)) (see in appendix). The next module is the calculation of the node scores used to detect the position of the optic disc. The graph nodes are numbered from top to bottom and left to right (Figure 4(b)) (see in appendix).

Next, the characteristics of the node (type: end or joint node, position) and the related information between the node and its neighbour (list of connected nodes above, list of connected nodes below) are needed. (Figure 4(c)) (see in appendix). The node's score is computed twice, traversing the graph from top to bottom and bottom to top.

a. The first is a top-down approach, assigning scores according to the following principles: the end node score (e) equals zero (see Figure 5) and the score of the joint node (j, parent). Score of the joint node is taken as the following condition from the score of the children that are the above-connected nodes, i) if the children have the same score, the parent's score is an increment of the child's score (see the following node ID: 5, 8, 10, 12, 19, 21 in Figure 5), ii) if the children's scores are not equal, the child's highest score belongs to the parent (see the following node ID: 7, 13, 14, 16, 20 in Figure 5), and iii) if the parent has only one child, the child's score is assigned to the parent (see the following node ID: 27, 28, 30, 33, 35 in Figure 5).

b. The second is to compute the graph node score using a bottom-up approach where the end node score is equal to zero. The joint node scoring is done in the opposite direction of the top-down approach where the below-connected nodes are the children.

c. The final score of the graph node is the minimum between the top-down score and the bottom-up score (Figure 5). The vascular root zone consists of k nodes (or a single node) with the highest final score.
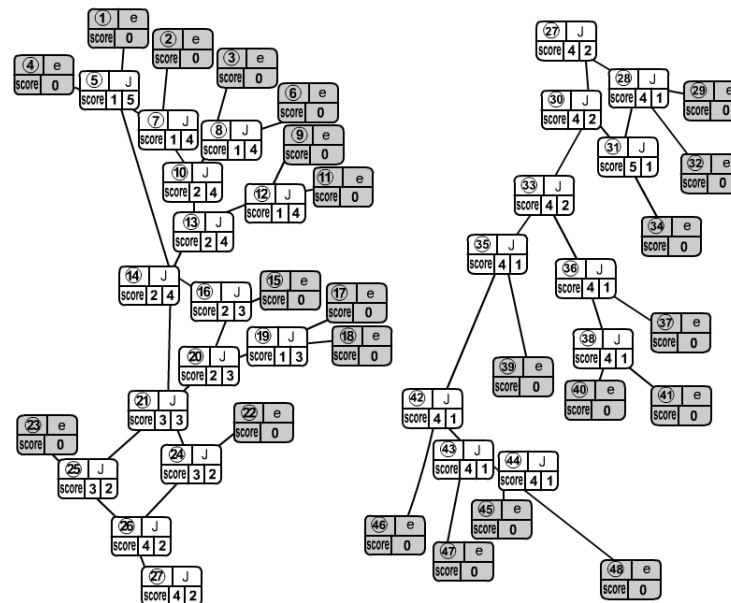

Figure 5. The node scores (left: top-down scores, right: bottom-up scores)

3. THE PROPOSED OD LOCALIZATION

The diagram in Figure 6 corresponds to significant stages in locating the optic disc. The method concept was based on structural modification and adaptation of blood vessels to generate information for the graph traversal algorithm. The details of the diagram are as follows:

a. The polar transformation converted a cartesian retinal image (Figure 7(a)) into interesting coordinates that provide a great view where parabolic blood vessels are characterized by vertical curves (Figure 7(b)). $f(\theta, r)$ represented the retinal image in polar coordinates, and the row and column indices indicated the angle and radius.
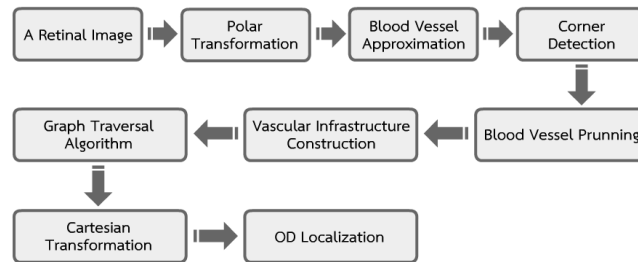
Figure 6. A diagram of the proposed OD localization

b. Applied the multi-scale and multi-orientation top hat filters (as in (3) and (4)) to a polar retinal image to segment the blood vessels preserving the optic nerve, central retina, and ophthalmic artery (Figures 8(a) and (b)).
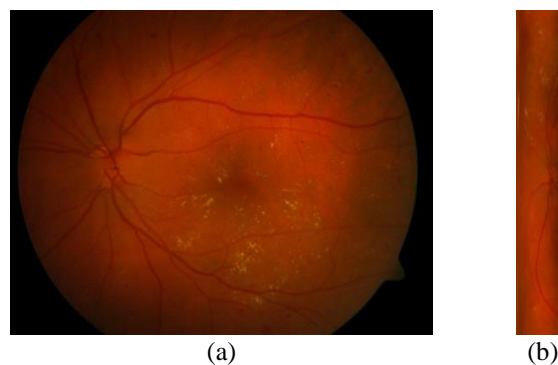

(a)   (b)

Figure 7. The retinal images (a) $f(x, y)$ and (b) $f(\theta, r)$
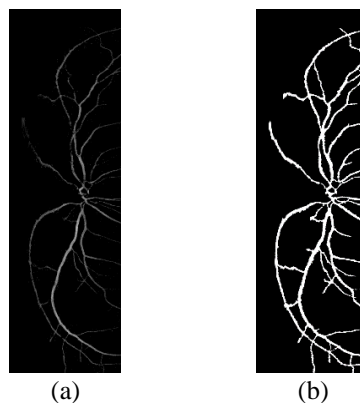

(a)   (b)

Figure 8. Blood vessel approximation (a) the filtered image and (b) the binary filtered image

c. Corner measurements using (5)-(9) revealed vascular branching and crossing patterns. The Harris score [8] (Figure 9(a)), combined with mathematical morphology, indicated the probability of corner structure along blood vessels (Figure 9(b)).

d. The vertical and horizontal projection algorithms of the corner image histogram removed capillaries. Probability analysis was used to calculate the histogram cutoff. A k% reduction in probability was monitored on the left and right sides of the peak (Figure 10(a)). The result of capillary removal provided a C-shaped band of blood vessels in the cartesian system (Figures 10(b) and (c)).
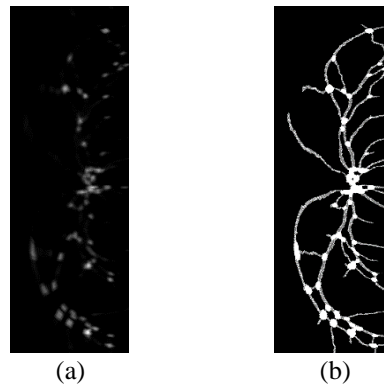
(a)   (b)

Figure 9. Corner detection (a) the Harris' scores and (b) the binary scores along blood vessels
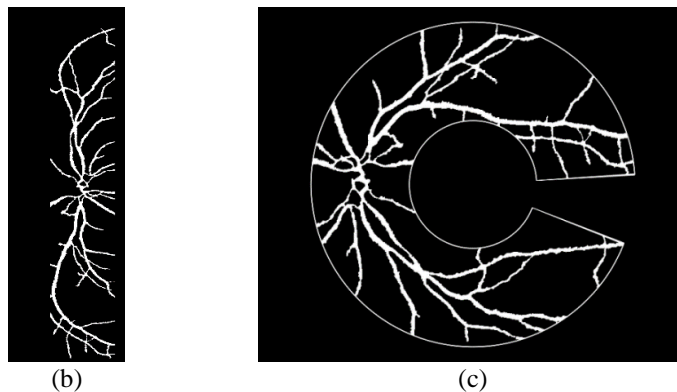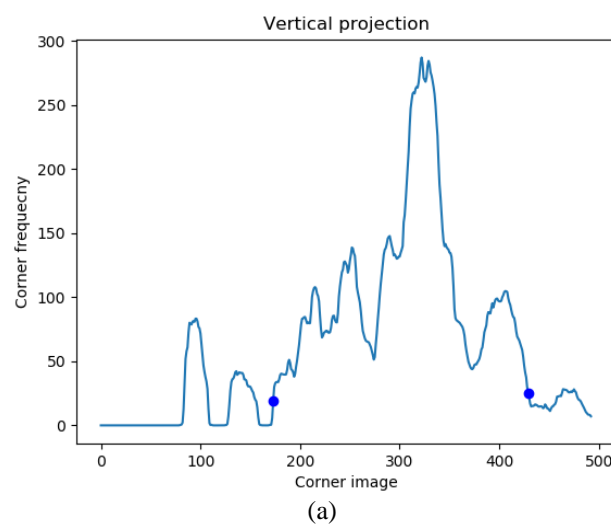

(a)

(b)   (c)

Figure 10. Blood vessel pruning (a) the vertical histogram projection of corner's scores with the cutoffs,
(b) capillaries removal, and (c) blood vessels in the C-shape band (a cartesian coordinate)

e. The next process was to apply the Zhang-Suen algorithm [17] to the C-shaped vascular band to create the vascular infrastructure (Figure 11(a)).

f. The proposed algorithm simulated a graph of vascular infrastructure. For graph nodes, the first thing involved was the classification of the type (end points or joint points) and the identification of the information (ID, position, type, lists of above and below connected nodes). The node traversal algorithm started from top to bottom and bottom to top to compute two scores of the graph node, then choosed the

minimum between the two scores as the node score. The root zone of the graph contained *n* nodes with the highest scores (Figure 11(b)).

g. Finally, the proposed algorithm located the optical disc at the center of the circle that exactly covers the root nodes in the cartesian system shown in Figures 12(a) and (b).
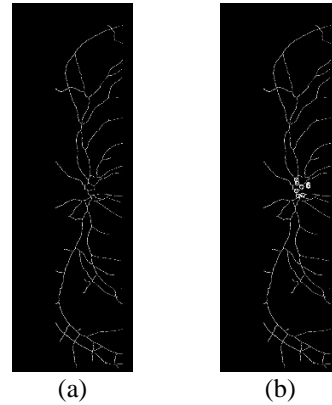

(a)   (b)

Figure 11. Vascular infrastructure with the root nodes, (a) infrastructure of blood vessels and (b) six nodes with the highest scores.

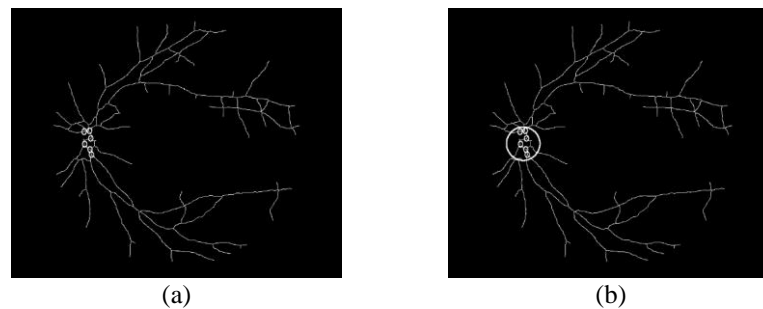(a)   (b)

Figure 12. The optic disc localization (a) the root nodes and (b) the centre of the circle covering the root nodes

4. MATERIALS AND EXPERIMENTAL RESULTS
4.1. Materials

In this paper, we obtained retinal images from five open source databases and evaluated the proposed method in which databases are the standard diabetic retinopathy database calibration level 0 (DIARETDB0) [18], the standard diabetic retinopathy database calibration level 1 (DIARETDB1) [19], the structured analysis of retina dataset (STARE) [11], the digital retinal images for vessel extraction (DRIVE) [20], and the method of evaluate of segmentation and indexing techniques in the field of retinal ophthalmology (MESSIDOR) [21]. All databases contained images of normal fundus and lesions such as microaneurysms and soft and hard exudates. In this study, the images from each database were separated into 2 classes according to the image situation and environment, the normal class (N) and the poor class (P). Two human observed manually classified the image classes from these image databases.

The normal class consisted of retinal images with prominent features such as high contrast, bright, round, and fully developed optic disc, as shown in Figure 13(a). The properties of the poor image class were clearly opposite to those of the normal image class, which is low contrast and has a disturbing shape of the optic disc, including a background imbalance shade (see Figure 13(b)). Furthermore, undesirable characteristics of bright lesions and noise acquisition appeared in both classes of retinal images. Table 1 detailed five open-source databases, including the classes of retinal images described.
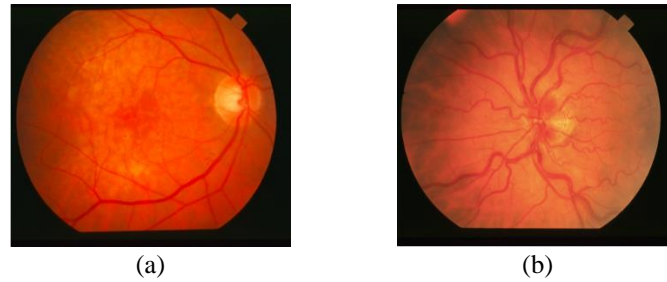
(a)   (b)

Figure 13. Image classes (a) a normal image and (b) a poor image

Table 1. Image classes for each image database

Database	DIARETDB0	DIARETDB1	STARE	DRIVE	MESSIDOR
Class N	112	75	58	34	1020
Class P	18	14	23	6	180
Total images	130	89	81	40	1200
Resolution	1500*1152	1500*1152	700*605	565*584	1140*960

4.2. Experimental results

In the evaluation, experimental accuracy was calculated as the percentage where the detected OD location was within the circumference of the ground truth in the reference standard. The performance of the proposed method was compared with 5 public methods. The first method was the 2D match filter-based algorithm proposed by Mahfouz and Fahmy [22] which its concept is to apply a 2D matching filter with multiple orientations to score the OD candidates for discovering the exact location of the OD. In Lu and Lim [23], the authors applied a line operator to capture OD from a circular luminosity structure. After evaluating the component changes with multiple aligned lines, the OD was determined based on the alignment of the maximum/minimum deviation lines. Ramakanth and Babu [24] proposed an approach that uses a single disk image as a reference or template and then used an approximate nearest neighbor map (ANNF) to identify the OD of the retinal image. The ANNF map generated the location of all patches closest to the patch in the reference image. Finally, patching the maximum likelihood map located the OD. The histogram matching method [25] consisted of two main processes: training and testing. The training procedure helped to simulate histogram templates for the red, green, and blue color spaces at the OD location. Similarity measurements of the histograms between training and testing images were used to improve procedural parameters and select the best template for discovering the OD position. The last method to be compared was a gravity law-based algorithm based on edge analysis [26]. The global thresholding techniques after edge detection produced both desired and undesired object contours. Then the unwanted contours were removed with a constant mask. Finally, the contour clusters were evaluated based on the mean distance to determine the exact OD location.

Tables 2 and 3 presented the percentage of optical disc localization accuracy, comparing the detected position with the OD centers of ground truth, where our algorithm provided the highest accuracy for both the normal and poor image classes. The proposed method obtained an average accuracy of 91.21% in DIARETDB0, 95.09% in DIARETDB1, 88.45% in STARE, 91.66% in DRIVE and 95.01% in MESSIDOR with the mean between the accuracy of the normal and the poor image cases. Finally, our method was able to achieve an average percentage accuracy of 92.28% for the five databases. In Table 2, most of the algorithms obtained a high percentage accuracy for all image databases according to the prominent characteristic of the optic disc as high-contrast, bright and complete round shape and the compared algorithm worked on these good properties to discover the OD position. Therefore, the limitations of these compared methods are poor illumination, darker OD with distorted shape, including bright lesions which provided low accuracy percentage (see Table 3).

Table 2. Percentage of the accuracy of the OD localization methods tested by the normal image class

Database	[22]	[23]	[24]	[25]	[26]	proposed method
DIARETDB0	97.31	98.21	98.21	94.07	96.42	99.10
DIARETDB1	93.33	94.66	93.33	90.66	93.33	97.33
STARE	86.2	86.2	94.26	72.41	77.58	94.31
DRIVE	100	100	100	97.05	97.05	100
MESSIDOR	97.84	98.13	97.94	92.35	93.43	98.92

Table 3. Percentage of the accuracy of the OD localization methods tested by the poor image class

Database	[22]	[23]	[24]	[25]	[26]	Proposed method
DIARETDB0	66.66	72.22	66.11	50	61.11	83.33
DIARETDB1	78.57	78.57	85.71	64.28	64.28	92.85
STARE	65.21	73.91	65.21	56.52	60.86	82.6
DRIVE	66.66	66.66	66.66	50	66.66	83.33
MESSIDOR	77.22	78.33	81.11	65.55	67.22	91.11

According to the symmetry of the retinal vasculature in a polar image, the position of the OD will be found using a graph traversal algorithm without considering the optic disc brightness and shape. The performance of the proposed method on the tested datasets, showing challenging factors such as pathology, low contrast, darker OD, and bright lesions, has been presented in Figures 14(a) to (e) which the OD position was shown by a black circle mark.

(a)   (b)   (c)

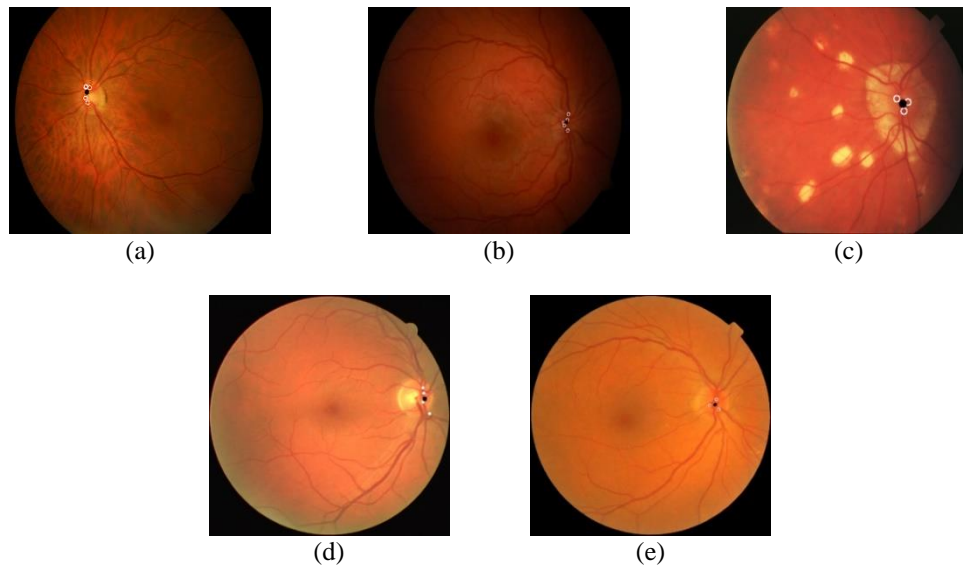(d)   (e)

Figure 14. The OD localization on the tested data sets (a) DIARETDB0, (b) DIARETDB1, (c) STARE, (d) DRIVE, and (e) MESSIDOR

5. CONCLUSION

An automated optic disc localization method has been proposed by incorporating the graph traversal algorithm and the vascular infrastructure of a retinal image in a polar coordinate. First, a new version of the top-hat filter applied the appropriate size and orientation of the elliptical structural elements to segment different blood vessels. Next, the capillaries were removed by histogram projection of the branching and crossing patterns of blood vessels. The vascular infrastructure was constructed to simulate a graph with nodes and edges. Finally, the algorithm traversed the graph nodes along the edges to calculate the node scores and discovered the root nodes that represent the position of the optical disc. The advantage of the proposed method is that do not depend on the prominent characteristics of the optical disc such as circular/elliptical shape, and brightness. The proposed OD localization was evaluated on five sets of retinal fundus images. Experimental results have shown that the proposed method performs well for healthy and complex retinal images.
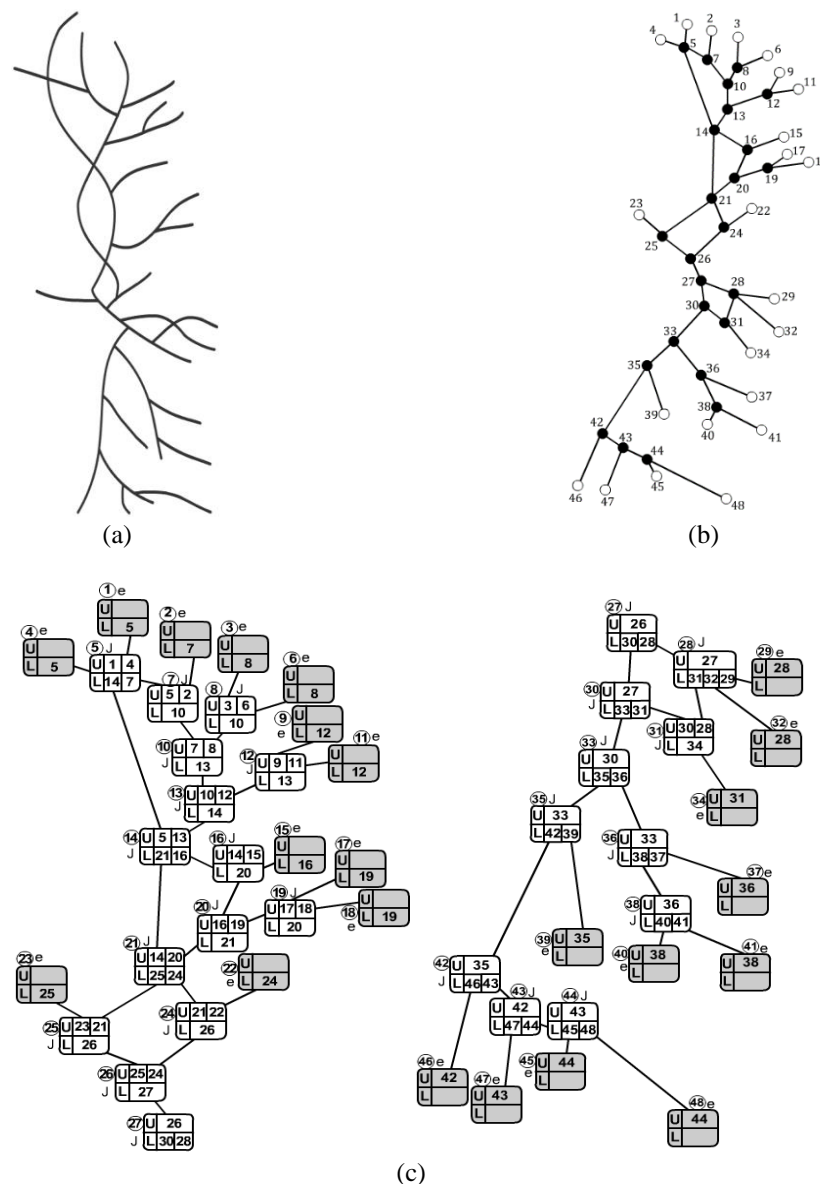
APPENDIX

Figure 4. The blood vessel graph (a) the vascular infrastructure, (b) the simulated graph with node ID, and (c) the node information

REFERENCES

[1]   G. Roglic, "WHO global report on diabetes," *World Health Organization*, vol. 1, no. 1, pp. 1–85, 2016.
[2]   M. N. Reza, "Automatic detection of optic disc in color fundus retinal images using circle operator," *Biomedical Signal Processing and Control*, vol. 45, pp. 274–283, Aug. 2018, doi: 10.1016/j.bspc.2018.05.027.
[3]   S. Lu, "Accurate and efficient optic disc detection and segmentation by a circular transformation," *IEEE Transactions on Medical Imaging*, vol. 30, no. 12, pp. 2126–2133, Dec. 2011, doi: 10.1109/TMI.2011.2164261.
[4]   H. Yu *et al.*, "Fast localization and segmentation of optic disk in retinal images using directional matched filtering and level sets," *IEEE Transactions on Information Technology in Biomedicine*, vol. 16, no. 4, pp. 644–657, Jul. 2012, doi: 10.1109/TITB.2012.2198668.
[5]   L. Xiong and H. Li, "An approach to locate optic disc in retinal images with pathological changes," *Computerized Medical Imaging and Graphics*, vol. 47, pp. 40–50, Jan. 2016, doi: 10.1016/j.compmedimag.2015.10.003.
[6]   B. Zou, C. Chen, C. Zhu, X. Duan, and Z. Chen, "Classified optic disc localization algorithm based on verification model," *Computers & Graphics*, vol. 70, pp. 281–287, Feb. 2018, doi: 10.1016/j.cag.2017.07.031.
[7]   J. E. Gutierrez, J. T. Barrena, M. Gamarra, P. R. Aroca, A. Valls, and D. Puig, "A color fusion model based on Markowitz portfolio optimization for optic disc segmentation in retinal images," *Expert Systems with Applications*, vol. 174, pp. 1–11, Jul. 2021, doi: 10.1016/j.eswa.2021.114697.
[8]   B. Gui, R. -J. Shuai, and P. Chen, "Optic disc localization algorithm based on improved corner detection," *Procedia Computer Science*, vol. 131, pp. 311–319, 2018, doi: 10.1016/j.procs.2018.04.169.

[9] M. Nergiz, M. Akın, A. Yıldız, and Ö. Takeş, "Automated fuzzy optic disc detection algorithm using branching of vessels and color properties in fundus images," *Biocybernetics and Biomedical Engineering*, vol. 38, no. 4, pp. 850–867, 2018, doi: 10.1016/j.bbe.2018.08.003.

[10] T. J. Jebaseeli, C. A. D. Durai, and J. D. Peter, "Retinal blood vessel segmentation from diabetic retinopathy images using tandem PCNN model and deep learning based SVM," *Optik*, vol. 199, pp. 1–12, Dec. 2019, doi: 10.1016/j.ijleo.2019.163328.

[11] A. D. Hoover, V. Kouznetsova, and M. Goldbaum, "Locating blood vessels in retinal images by piecewise threshold probing of a matched filter response," *IEEE Transactions on Medical Imaging*, vol. 19, no. 3, pp. 203–210, Mar. 2000, doi: 10.1109/42.845178.

[12] G. Sun, X. Liu, S. Wang, L. Gao, and M. Liu, "Width measurement for pathological vessels in retinal images using centerline correction and k-means clustering," *Measurement*, vol. 139, pp. 185–195, Jun. 2019, doi: 10.1016/j.measurement.2019.03.005.

[13] S. Roychowdhury, D. Koozekanani, and K. Parhi, "Blood vessel segmentation of fundus images by major vessel extraction and sub-image classification," *IEEE Journal of Biomedical and Health Informatics*, vol. 19, no. 13, pp. 1–11, 2015, doi: 10.1109/JBHI.2014.2335617.

[14] X. Wang, X. Jiang, and J. Ren, "Blood vessel segmentation from fundus image by a cascade classification framework," *Pattern Recognition*, vol. 88, pp. 331–341, Apr. 2019, doi: 10.1016/j.patcog.2018.11.030.

[15] M. N. Zahoor and M. M. Fraz, "Fast optic disc segmentation in retina using polar transform," *IEEE Access*, vol. 5, pp. 12293–12300, 2017, doi: 10.1109/ACCESS.2017.2723320.

[16] K. K. Delibasis, A. I. Kechriniotis, C. Tsonos, and N. Assimakis, "Automatic model-based tracing algorithm for vessel segmentation and diameter estimation," *Computer Methods and Programs in Biomedicine*, vol. 100, no. 2, pp. 108–122, Nov. 2010, doi: 10.1016/j.cmpb.2010.03.004.

[17] W. A. Ain, S. N. H. S. Abdullah, B. Bataineh, T. A. Ain, and K. Omar, "Skeletonization algorithm for binary images," *Procedia Technology*, vol. 11, pp. 704–709, 2013, doi: 10.1016/j.protcy.2013.12.248.

[18] T. Kauppi, V. Kalesnykiene, J. Kamarainen, L. Lensu, and I. Sorri, "DIARETDB0: evaluation database and methodology for diabetic retinopathy algorithms," *Computer Science and Medicine*, pp. 1–17, 2007.

[19] T. Kauppi *et al.*, "DIARETDB1 diabetic retinopathy database and evaluation protocol," in *Procedings of the British Machine Vision Conference 2007*, 2007, pp. 61–65, doi: 10.5244/C.21.15.

[20] J. Staal, M. D. Abramoff, M. Niemeijer, M. A. Viergever, and B. van Ginneken, "Ridge-based vessel segmentation in color images of the retina," *IEEE Transactions on Medical Imaging*, vol. 23, no. 4, pp. 501–509, Apr. 2004, doi: 10.1109/TMI.2004.825627.

[21] E. Decencière *et al.*, "Feedback on a publicly distributed database: the messidor database," *Image Analysis & Stereology*, vol. 33, no. 3, pp. 231–234, Aug. 2014, doi: 10.5566/ias.1155.

[22] A. E. Mahfouz and A. S. Fahmy, "Fast localization of the optic disc using projection of image features," *IEEE Transactions on Image Processing*, vol. 19, no. 12, pp. 3285–3289, Dec. 2010, doi: 10.1109/TIP.2010.2052280.

[23] S. Lu and J. H. Lim, "Automatic optic disc detection from retinal images by a line operator," *IEEE Transactions on Biomedical Engineering*, vol. 58, no. 1, pp. 88–94, Jan. 2011, doi: 10.1109/TBME.2010.2086455.

[24] S. A. Ramakanth and R. V. Babu, "Approximate nearest neighbour field based optic disk detection," *Computerized Medical Imaging and Graphics*, vol. 38, no. 1, pp. 49–56, Jan. 2014, doi: 10.1016/j.compmedimag.2013.10.007.

[25] A. Dehghani, H. A. Moghaddam, and M. -S. Moin, "Optic disc localization in retinal images using histogram matching," *EURASIP Journal on Image and Video Processing*, vol. 1, pp. 1–11, Dec. 2012, doi: 10.1186/1687-5281-2012-19.

[26] M. Alshayeji, S. A. A-. Roomi, and S. Abed, "Optic disc detection in retinal fundus images using gravitational law-based edge detection," *Medical & Biological Engineering & Computing*, vol. 55, no. 6, pp. 935–948, Jun. 2017, doi: 10.1007/s11517-016-1563-0.

BIOGRAPHIES OF AUTHORS

Annupan Rodtook received the M.Sc. in Computer Science from Mongkut's Institute of Technology Ladkrabang of Thailand in 1996. He has received his Ph.D. degree in Technology from Sirindhorn International Institute of Technology, Thammasat University of Thailand in 2005. He is currently Associate Professor at the Computer Science Department, Ramkhamhaeng University of Thailand. His research interests include image processing, medical image processing and pattern recognition. He can be contacted at email: annupan@rumail.ru.ac.th.

Sirikan Chucherd received the B.E. and M.E. degrees in electrical engineering from King Mongkut's Institute of Technology Ladkrabang of Thailand in 1998 and 2001 respectively. She has received her Ph.D. degree in Computer Science from Sirindhorn International Institute of Technology, Thammasat University of Thailand in 2011. She is currently Assistant Professor at School of Information Technology, Mae Fah Luang University of Thailand. Her research interests include medical image processing and pattern recognition. She can be contacted at email: sirikan@mfu.ac.th.